1   # GPI-anchored Gas1 protein regulates cytosolic proteostasis in yeast

2   **Authors:** Yuhao Wang[1,2], Linhao Ruan[1], Rong Li[1,3*]

3   **Affiliations:**

4   [1]Center for Cell Dynamics and Department of Cell Biology, Johns Hopkins University School of

5   Medicine; Baltimore, MD 21205, USA.

6   [2]Biochemistry, Cellular and Molecular Biology (BCMB) Graduate Program, Johns Hopkins

7   University School of Medicine; Baltimore, MD 21287, USA.

8   [3]Mechanobiology Institute and Department of Biological Sciences, National University of

9   Singapore; Singapore 117411, Singapore.

10   [*]Corresponding author. Email: rong@jhu.edu

11

Abstract

13   Decline in protein homeostasis (proteostasis) is a hallmark of cellular aging and aging-related

14   diseases. Maintaining a balanced proteostasis requires a complex network of molecular

15   machineries that govern protein synthesis, folding, localization, and degradation. Under

16   proteotoxic stress, misfolded proteins that accumulate in cytosol can be imported into

17   mitochondria for degradation via 'mitochondrial as guardian in cytosol' (MAGIC) pathway. Here

18   we report an unexpected role of yeast Gas1, a cell wall-bound glycosylphosphatidylinositol

19   (GPI)-anchored β-1,3-glucanosyltransferase, in differentially regulating MAGIC and ubiquitin-

20   proteasome system (UPS). Deletion of Gas1 inhibits MAGIC but elevates polyubiquitination and

21   UPS-mediated protein degradation. Interestingly, we found that Gas1 exhibits mitochondrial

22   localization attributed to its C-terminal GPI anchor signal. But this mitochondria-associated GPI

23   anchor signal is not required for mitochondrial import and degradation of misfolded proteins via

24   MAGIC. By contrast, catalytic inactivation of Gas1 via the $gas1^{E161Q}$ mutation inhibits MAGIC

25   but not its mitochondrial localization. These data suggest that the glucanosyltransferase activity

26   of Gas1 is important for regulating cytosolic proteostasis.

27

Introduction

29   Many aging-related degenerative diseases are associated with loss of proteostasis characterized

30   by protein misfolding and formation of protein aggregates (1-3). Major protein quality control

31   pathways such as UPS and autophagy play essential roles in clearance and turnover of misfolded

32   proteins (4). Mitochondria are key organelles not only in cellular metabolism (5) but also in

33   clearing misfolded proteins via a process termed as 'mitochondrial as guardian in cytosol'

34   (MAGIC) (6-8). In budding yeast, misfolded cytosolic proteins can translocate into mitochondria

35 through mitochondrial import channels (6). The yeast Lon protease, Pim1, is involved in the

36 degradation of imported misfolded proteins in the mitochondrial matrix, which in turn facilitates

37 the dissolution of cytosolic protein aggregates associated with mitochondria (6,7). Likewise, a

38 model unstable cytosolic protein (FlucDM) can be imported into the mitochondrial matrix of

39 human RPE-1 cells (6). Proteasomal inhibition by MG132 in HeLa cells can induce the import of

40 unfolded cytosolic GFP into mitochondria through the joint action of mitochondrial outer

41 membrane protein FUNDC1 and cytosolic chaperone HSC70 (9). Many disease-related proteins

42 such as α-synuclein, FUS, and TDP-43 have been shown to accumulate in mitochondria of

43 various human cell models and influence mitochondrial fitness (10-12). These findings suggest

44 that MAGIC may be a conserved process that connects cytosolic proteostasis with mitochondrial

45 functions.

46

47 To elucidate the molecular mechanism and regulation of MAGIC in yeast, we conducted an

48 unbiased genetic screen using the non-essential yeast knockout library that unveiled potential

49 regulators of MAGIC including Gas1 (7). Gas1 (glycophospholipid-anchored surface protein 1)

50 is a β-1,3-glucanosyltransferase anchored to the outer leaflet of the plasma membrane via a GPI

51 moiety and crosslinked with the cell wall (13-16). Gas1 elongates the β-1,3-glucan chains and

52 plays an important role in expansion and remodeling of the cell wall (17). Here, we show that

53 Gas1 is a positive regulator of MAGIC, and loss of Gas1 prevents the accumulation and

54 degradation of misfolded proteins in mitochondria. We also provide insights into the subcellular

55 localization of Gas1-GFP by showing that its C-terminal GPI anchor signal, but not the main part

56 of the protein, localizes to mitochondria. Despite this atypical localization, the catalytic activity

57 of Gas1, but not the mitochondria-associated GPI anchor signal, is required for maintaining

3

58   MAGIC. Furthermore, two other cell wall mutants show moderate inhibition of MAGIC,

59   suggesting that maintenance of cell wall integrity in general may be important for MAGIC. In

60   addition to altered MAGIC phenotypes, Gas1-deficient cells exhibit elevated protein

61   polyubiquitination and UPS-mediated degradation of an N-end rule substrate (Ub-R-EGFP).

62   Taken together, our work identifies an unexpected role of Gas1 in regulating proteostasis

63   pathways and suggests an underappreciated connection between cytosolic proteostasis and cell

64   wall integrity.

65

66   **Results**

67   **Gas1 is required for mitochondrial accumulation and degradation of misfolded proteins**

68   We conducted an unbiased genetic screen and subsequent validations that uncovered potential

69   MAGIC regulators in yeast by performing the split-GFP assay in the yeast non-essential

70   knockout library (6,7). In brief, cytosolic proteins such as Lsg1, an endogenous aggregation-

71   prone protein (6), or FlucSM, a destabilized firefly luciferase mutant and a sensor of the

72   proteostasis stress (6,7,18), were tagged with the eleventh β-strand of GFP (GFP_{11}), and the first

73   ten β-strands of GFP (GFP_{1-10}) were targeted to mitochondrial matrix by fusing with the

74   mitochondrial matrix protein Grx5 (Grx5-GFP_{1-10}) or the mitochondrial targeting sequence of

75   Subunit 9 of mitochondrial ATPase (Su9 MTS) from *Neurospora crassa* (MTS-mCherry-GFP_{1-}

76    $_{10}$). In wild-type cells, proteotoxic stresses such as heat shock (6) or acute overexpression of

77   misfolded proteins induced by estradiol (7) resulted in an increased GFP fluorescence (spGFP

78   signal) within mitochondria (Figure 1A-C). We analyzed each mutant before and after stress and

79   identified gene deletions that gave rise to differential spGFP patterns compared to the wild-type

80   cell (7).

81

82   *Δgas1* was one of mutants that failed to show an increased FlucSM spGFP signal after stress

83   compared to the wild-type control (Figure 1B and C) (7). Because activation of Snf1 kinase, the

84   yeast homolog of human AMP-activated protein kinase, inhibits the import of misfolded proteins

85   into mitochondria (7), we first asked if Snf1 activity is elevated in *Δgas1* by using the nuclear-

86   cytoplasmic transport of Mig1-GFP as a reporter. Under glucose restriction, Mig1 is

87   phosphorylated by active Snf1 and exported from the nucleus (7,19). However, Mig1-GFP signal

88   remained in the nucleus in *Δgas1* mutant cells and even exhibited slightly more enrichment

89   compared to the control (Figure 1D and E). This data argues against the possibility that the

90   inhibition of MAGIC in *Δgas1* mutant was primarily caused by Snf1 activation. In addition to

91   the reduced FlucSM spGFP signal, we used immunoblots to assess the degradation of misfolded

92   proteins, and performed time-lapse imaging to track the disaggregation of cytosolic protein

93   aggregates, both of which have been shown to depend on MAGIC (6). We found that the post-

94   heat shock degradation of Lsg1 was significantly delayed in *Δgas1* (Figure 1F and G). The

95   dissolution of protein aggregates labeled with protein disaggregase Hsp104-GFP after heat shock

96   was also impaired, even though the association of aggregates with mitochondria appeared

97   unaffected (Figure 1H and I). In sum, these data suggest that Gas1 is a regulator of the

98   mitochondria-mediated pathway for degrading certain cytosolic aggregation-prone proteins.

99

5

Re-analysis of the intracellular localization of Gas1-GFP reveals an unexpected

mitochondrial targeting domain

Gas1 was previously shown to localize to mitochondria in addition to cell periphery and ER

(20,21). It was therefore reasonable for us to hypothesize that the mitochondrial localization of

Gas1 is related to its role in MAGIC. To test this, it was necessary to gain an understanding of

how this purported cell wall protein is targeted to mitochondria. By using confocal microscopy

to observe the subcellular localization of the C-terminally tagged Gas1-GFP, we confirmed that a

portion of GFP fluorescence colocalized with mitochondria labeled with MTS-mCherry, while

the other fraction of GFP fluorescence appeared to be in the ER and nuclear periphery (Figure

2A), which was reported previously (21). By using super-resolution microscopy, we found that

mitochondrial Gas1-GFP signal delineates the contour of the mitochondrial matrix, suggesting its

localization in the mitochondrial membranes or intermembrane space (Figure 2B). Importantly,

our Gas1-GFP strain was resistant to treatment with calcofluor white (CFW), a cell wall

destabilizing reagent (22), whereas _Δgas1_ mutant with cell wall defects failed to grow on CFW-

containing plates (Supplementary Figure 1A). This data suggests that C-terminal GFP tagging of

Gas1 preserves its function in maintaining cell wall integrity.

The trafficking and post-translational modification of Gas1 are intricately coupled processes (13-

15,23,24). To reach the cell surface, newly synthesized Gas1 protein is targeted to ER by a

canonical N-terminal signal sequence (SS) (13-15). A cleavable hydrophobic sequence at the C

terminus temporarily anchors Gas1 on the ER membrane and serves as a GPI anchor signal

(GPI*) that is necessary for the addition of a GPI moiety via the GPI-anchor transamidase

complex (13,15,23). As a result, we conceived that the cleaved GPI* should bear the GFP tag

123   (GPI*-GFP), and the GPI-anchored Gas1 (Gas1-GPI) is transported to plasma membrane

124   through the secretory pathway where it is progressively modified by N-glycosylation and O-

125   glycosylation in the ER and Golgi (13,23) (Figure 2C). In line with this model, anti-GFP

126   immunoblot analysis on the yeast whole cell lysate of Gas1-GFP strain showed two major

127   species (Figure 2D). A higher molecular weight (MW) species exhibited the expected size of N-

128   glycosylated uncleaved Gas1-GFP (~120 kDa), as confirmed by treatment with tunicamycin, an

129   inhibitor of N-acetylglucosamine transferases (25), which decreased its MW to the unmodified

130   Gas1-GFP (~90 kDa) (Figure 2D and E). By contrast, dithiothreitol (DTT) treatment, which

131   reduces disulfide bonds of ER proteins and causes the unfolded protein stress (26), had no effect

132   on N-glycosylation (Figure 2E). The low MW species appeared to be comparable to GPI*-GFP

133   (~28 kDa) (Figure 2D). Interestingly, either treatment with tunicamycin or DTT reduced the

134   amount of low MW species, suggesting that ER stress may compromise the cleavage of GPI*

135   regardless of the presence of N-glycosylation (Figure 2E).

136

137   We next tested if the cleavage of GPI* is responsible for the mitochondrial localization of Gas1.

138   The amino acid sequence at and adjacent to the GPI anchor attachment site of Gas1 (N528) is

139   important for efficient peptide cleavage (24) (Supplementary Figure 1B). Mutation of N528 to a

140   lysine residue (N528K) abolishes the glycolipid transfer and peptide cleavage, and as a result,

141   Gas1 remains unprocessed and only N-glycosylated in the ER (24). We found that Gas1[N528K]-

142   GFP failed to exhibit any mitochondrial localization (Figure 2F), and as expected the low MW

143   species also disappeared in the anti-GFP immunoblot (Figure 2G). This result indicates that

144   mitochondrial GFP fluorescence requires the cleavage of GPI*.

145

146 To differentially observe the N and C terminal portion of Gas1 after GPI* cleavage, we fused the

147 Gas1 protein with a mCherry at its N terminus after the ER-targeting signal peptide, and

148 simultaneously with a GFP at its C terminus following the GPI anchor signal (mCherry-Gas1-

149 GFP). The mCherry signal was mostly detected on the cell periphery where the GFP

150 fluorescence was largely absent, whereas only GFP but not mCherry signal was detected on

151 mitochondria (Figure 2H). Only at the ER/nuclear periphery were both mCherry and GFP

152 colocalized, which likely represented the unprocessed Gas1 (Figure 2H). This dual-color pattern

153 further confirms that after GPI* cleavage, the N-terminal main portion of the protein is trafficked

154 to the cell periphery whereas GPI* is targeted to mitochondria.

155

156 To determine if GPI* is sufficient for mitochondrial localization, we ectopically expressed the C-

157 terminally tagged GPI*-GFP with or without an additional N-terminal ER-targeting signal

158 sequence (SS-GPI*-GFP) under a native *GAS1* promoter. GPI*-GFP signal was predominantly

159 localized to mitochondria, whereas SS-GPI*-GFP showed both ER and mitochondrial

160 localization (Figure 2I and J). This data suggests that the GPI anchor signal of Gas1 could be a

161 mitochondrial targeting sequence even in the presence of an ER-targeting sequence.

162

163 **Enzymatic activity of Gas1 rather than its GPI anchor signal is required for MAGIC**

164 We next asked if the mitochondrial localized GPI anchor signal of Gas1 is required for

165 maintaining MAGIC, a process dependent on functional mitochondrial import (6). To avoid

166 affecting the targeting to plasma membrane and function of Gas1 in the cell wall, we replaced the

167 endogenous GPI anchor signal of Gas1 by that of Gas3 and Gas5, two closely related Gas family

8

168   glucanosyltransferases with C-terminal GPI anchor signals (Supplementary Figure 1B) (15).

169   Yeast strains expressing recombinant proteins (Gas1-GPI*$_{Gas3}$ and Gas1-GPI*$_{Gas5}$) were resistant

170   to treatment with CFW, and these proteins were fully glycosylated at a level comparable to the

171   wild-type Gas1 (Supplementary Figure 1C and D), indicating normal processing and cell wall

172   function of the recombinant Gas1. Importantly, by C-terminal tagging with GFP, neither

173   recombinant protein exhibited mitochondrial localization: Gas1-GPI*$_{Gas3}$-GFP was largely

174   confined to the ER, and Gas1-GPI*$_{Gas5}$-GFP signal appeared to be modestly present in the

175   vacuole (Figure 3A). Mitochondrial accumulation of misfolded FlucSM after acute

176   overexpression was not affected by GPI* replacement (Figure 3B and C). Misfolded endogenous

177   Lsg1 was also degraded normally after heat shock (Figure 3D and E). These results suggest that

178   the GPI anchor signal of Gas1 and its mitochondrial localization are not involved in the

179   regulation of MAGIC.

180

181   We therefore tested if the glucanosyltransferase activity of Gas1 is required for MAGIC by

182   studying the effect of the catalytically inactive *gas1^{E161Q}* mutation (21,27), which also caused

183   CFW sensitivity (Supplementary Figure 1E). Like the wild-type protein, Gas1^{E161Q} was fully

184   glycosylated and likely trafficked to the cell surface (Supplementary Figure 1F). Gas1^{E161Q}-GFP

185   showed both ER and mitochondrial GFP localization, indicative of normal cleavage of GPI*

186   (Figure 4A). But like *Δgas1*, this mutant exhibited defects in proteostasis and MAGIC, including

187   delayed dissolution of protein aggregates after heat shock and reduced accumulation of

188   misfolded FlucSM in mitochondria (Figure 4B-E). These results suggest that the enzymatic

189   activity of Gas1 is essential for MAGIC.

190

191   To determine whether loss of cell wall integrity could inhibit MAGIC in general, we examined

192   two other cell wall mutants with the deletion of *BGL2* encoding endo-β-1,3-glucanase Bgl2 (28),

193   or *GAS5* encoding another β-1,3-glucanosyltransferase (14,15). Both mutants showed sensitivity

194   to CFW, albeit much milder than *Δgas1* (Supplementary Figure 1G). They also caused a

195   moderate reduction in mitochondrial accumulation of FlucSM in spGFP assay (Supplementary

196   Figure 1H), which was less severe than Gas1-deficient cells (*Δgas1* in Figure 1C; *gas1^{E161Q}* in

197   Figure 4E). This analysis indicates that cell wall maintenance is indeed important for MAGIC.

198

199   **Effect of Gas1 deficiency on UPS**

200   To gain insights into whether Gas1 plays a broader role in other proteostasis pathways, we

201   examined the effect of *Δgas1* on UPS. Surprisingly, anti-ubiquitin immunoblot analysis on the

202   whole cell lysate of the mutant revealed a drastic increase in overall protein polyubiquitination

203   compared to the wild-type cell (Figure 4F). Over-accumulated polyubiquitinated proteins

204   gradually disappeared after inhibiting protein synthesis by cycloheximide (Figure 4F). In contrast

205   to the delayed degradation of MAGIC substrate, loss of Gas1 resulted in a faster degradation of

206   non-misfolded Ub-R-EGFP, an N-end rule substrate of the ubiquitin-proteosome system (Figure

207   4G and H) (29-31). In summary, our data suggests that loss of Gas1 activity may enhance UPS

208   while inhibiting MAGIC.

209

210   **Discussion**

211   Yeast Gas1 is a GPI-anchored β-1,3-glucanosyltransferase that elongates the β-1,3-glucan chains

212   and plays a critical role in the dynamic remodeling of the cell wall (14,15). The yeast null mutant

10

213   (*Δgas1*) shows cell wall defects characterized by round cells, CFW sensitivity, reduced growth

214   rate, and decreased cell viability during the stationary phase (22,32,33). Gas1 deficiency also

215   triggers the cell wall integrity signaling pathway and compensatory responses such as an increase

216   in chitin synthesis and deposition to rescue cell wall integrity (32,34). In addition to the

217   established function at the cell wall, Gas1 was shown to play roles in intracellular processes such

218   as DNA damage response (35), locus-specific transcriptional silencing (21), and ER stress

219   response (36). Deletion of Gas1 increases cellular sensitivity to DNA damages caused by

220   genotoxins (35), and loss of its enzymatic activity leads to defective telomeric silencing and

221   elevated rDNA silencing (21). Because C-terminally tagged Gas1-GFP shows intracellular

222   localizations in ER/nuclear periphery (as well as mitochondria) (20,21), it has been proposed that

223   Gas1 is involved in post-translational glycosylation of putative chromatin components (21,35).

224   Loss of Gas1 also elevates the unfolded protein response (UPR) pathway and renders the mutant

225   cells resistant to tunicamycin-induced ER proteotoxic stress (36). Both UPR and ER-associated

226   degradation (ERAD) maintain proteostasis in the ER and may in turn promote the secretion and

227   glycosylation of essential plasma membrane and cell wall proteins (37). However, detailed

228   mechanisms underlying the intracellular functions of Gas1 remain unclear.

229

230   Mitochondria are important organelles in cellular metabolism and cytosolic proteostasis (5-9,38).

231   Loss of cytosolic proteostasis is manifested by protein misfolding and formation of protein

232   aggregates, which are often tethered to intracellular organelles such as ER and mitochondria

233   (39,40). Under proteotoxic stress, certain misfolded cytosolic proteins can be translocated into

234   and degraded inside mitochondria through MAGIC pathway (6). Our data suggests that Gas1

235   function is important for cytosolic proteostasis mechanisms including MAGIC and UPS.

11

236 Specifically, Gas1 deficiency inhibits the mitochondrial accumulation and degradation of

237 aggregation-prone proteins but promotes UPS-mediated degradation of a non-misfolded N-end

238 rule substrate. One caveat of this study is that most of our observations were based on a few

239 model substrates such as FlucSM, Lsg1, and Ub-R-EGFP. Thus the generality and the underlying

240 mechanisms of our observations are presently unknown.

241

242 While investigating if mitochondrial targeting is important for the role of Gas1 in MAGIC, we

243 unexpectedly identified the C-terminal GPI anchor signal of Gas1 (GPI*$_{Gas1}$) as an

244 unconventional mitochondrial targeting sequence. GPI*$_{Gas1}$ does not bear typical amphiphilic

245 helices like Su9 MTS from *Neurospora crassa* but likely contains a transmembrane domain,

246 which was not present in GPI*$_{Gas3}$ or GPI*$_{Gas5}$ (Supplementary Figure 2A). It is worth noting that

247 a previous study showed that GPI*$_{Gas1}$ with an N-terminal GFP tag (also denoted as GFP-

248 Gas1GPI) only exhibits ER localization (41). We speculate that a well-folded GFP at the N

249 terminus may hinder the import or association of GPI* with mitochondria. GPI* may have a dual

250 targeting specificity that allows its route to ER when mitochondrial targeting is impaired. Anti-

251 GPI*$_{Gas1}$ immunoblots on mitochondrial fraction or immunofluorescence staining may be

252 necessary to further validate its subcellular localization. Also, it will be interesting to test if some

253 other GPI-anchored proteins in yeast or higher organisms contain a GPI anchor signal with

254 similar hydrophobic properties and mitochondrial targeting capacity.

255

256 By replacing the GPI* of Gas1 by that of Gas3 or Gas5, we showed that this mitochondria-

257 associated peptide is dispensable for mitochondrial accumulation of misfolded FlucSM and post-

12

258 heat shock degradation of Lsg1 by MAGIC. By contrast, the catalytically inactive Gas1^{E161Q}

259 protein exhibited normal maturation and mitochondrial localization, but still failed to maintain

260 MAGIC. Importantly, two other cell wall mutants with moderate CFW sensitivity also displayed

261 mild inhibition of MAGIC, suggesting that cell wall integrity may be important for MAGIC. The

262 stronger phenotypes of $\Delta gas1$ or $gas1^{E161Q}$ mutant than others in terms of CFW sensitivity and

263 MAGIC inhibition may be attributed to either more severe cell wall defects or Gas1-specific

264 effects that remain to be determined. One possibility is that loss of cell wall associated Gas1

265 activity may trigger the downstream signaling pathways that separately or jointly regulate

266 MAGIC and UPS. Our results, however, do not rule out the possibility that the intracellular

267 fraction of Gas1 in the ER/nuclear periphery plays a more direct role in proteostasis.

268

269 **Materials and Methods**

270 **Yeast strains and growth conditions**

271 Yeast strains used in this study are based on the BY4741 strain background and listed in Table 1.

272 Gene deletion and protein tagging were performed by using PCR-mediated homologous

273 recombination and verified by PCR genotyping. *GAS1-GFP* and *MIG1-GFP* strain were

274 obtained from the yeast GFP clone collection (20). *PUS1-RFP* strain was retrieved from yeast

275 RFP library (42). $\Delta bgl2$ and $\Delta gas5$ were collected from the non-essential yeast knockout library

276 (43). For the FlucSM split-GFP assay, GFP$_{1-10}$ was fused with the mitochondrial matrix protein

277 Grx5 under *GPD* promoter and stably integrated into yeast genome at the *TRP1* locus. FlucSM-

278 HA-GFP$_{11}$ (6) under *GAL1* promoter and GEM transcriptional factor (44) were cloned and stably

279 integrated into yeast genome. Mitochondria were labeled with Tom70-mCherry in the split-GFP

280 assay or with MTS-mCherry in other imaging experiments.

13

281

282   To construct $gas1^{N528K}$ and $gas1^{E161Q}$ mutants with a GFP tag, Gas1-GFP was cloned into a

283   plasmid, and underwent site-directed mutagenesis, before stably integrated into the *HO* locus. To

284   construct $gas1^{E161Q}$ mutants for the spotting assay, split-GFP assay, and imaging of protein

285   aggregates, a plasmid containing $gas1^{E161Q}$ was linearized and integrated into the *kanMX6* locus

286   of the corresponding *Δgas1* strain. For the dually labeled mCherry-Gas1-GFP strain, mCherry-

287   Gas1 and mCherry-Gas1-GFP was cloned and integrated into the *HO* locus of *Δgas1* strain. The

288   last 31 residues of Gas1 after the cleavage site (GPI*) were fused with a GFP at the C terminus

289   to construct the GPI*-GFP, and the ER-targeting signal peptide of Gas1 was added to the N

290   terminus to construct the SS-GPI*-GFP. To replace the GPI* sequence of endogenous *GAS1*, the

291   GPI anchor signal sequence of *GAS3* (last 26 residues) or *GAS5* (last 22 residues) together with a

292   *kanMX6* selective cassette was amplified from corresponding plasmids in the Molecular

293   Barcoded Yeast (MoBY) ORF Library (45) and inserted into the *GAS1* gene right after the

294   sequence of N528 residue. Replacements were validated by colony PCR and sequencing. All

295   variants of *GAS1* were expressed under *GAS1* promoter. Ub-R-EGFP under *CUP1* promoter was

296   cloned from the plasmid pYES2-Ub-R-EGFP (Addgene #11953) (29) and stably integrated into

297   the *TRP1* locus.

298

299   Standard YEP (yeast extract-peptone) supplemented with 2 % glucose (YPD) was used for

300   transformations, biochemical analyses, and spotting assays. Synthetic complete (SC)

301   supplemented with 2 % glucose was used for growing cells for confocal and super-resolution

302   imaging. Yeast culture and plates were incubated at 30 °C except during heat shock at 42 °C.

303   Optical density at 600 nm (OD_{600}) was used to estimate the amount of yeast cells used in the

304   various experiments.

305

Drug treatments

307   β -estradiol (E2758, MilliporeSigma) was dissolved in ethanol and added to a final concentration

308   of 1 μM for 90 min. Tunicamycin (T7765, MilliporeSigma) was dissolved in DMSO and used at

309   a final concentration of 10 μg/ml for 2 h. DTT (R0861, Thermo Fisher) was dissolved in H_2O

310   and added into the yeast cell cultures at a final concentration of 10 mM for 2 h. Cycloheximide

311   (239764, MilliporeSigma) was dissolved in DMSO and 100 μg/ml was used to treat cells for the

312   indicated period. Calcofluor white (F3543, MilliporeSigma) was dissolved in DMSO to 10

313   mg/ml as stock and added in autoclaved YPD media plus 2 % agar at a final concentration of 10

314   μg/ml before agar solidification. $CuSO_4$ (C1297, MilliporeSigma) was dissolved in H_2O and 1

315   mM was used to treat cells for 30 min.

316

Confocal microscopy and imaging conditions

318   Live cell images were acquired using a Yokogawa CSU-10 spinning disc on the side port of a

319   Carl Zeiss 200 m inverted microscope. Laser 488 or 561 nm excitation was applied to excite

320   GFP or mCherry, respectively, and the emission was collected through the appropriate filters

321   onto a Hamamatsu C9100-13 EMCCD on the spinning disc confocal system. Regarding the

322   multi-track acquisition, the configuration of alternating excitation was used to avoid the bleed-

323   through of GFP. The spinning disc was equipped with a 100×1.45 NA Plan-Apochromat

324   objective.

15

325

326   Yeast culture condition for imaging: yeast cells were cultured in SC plus 2 % glucose overnight

327   at 30 °C. The cells were then refreshed in the corresponding media for at least 3 hours at 30 °C

328   until reaching an OD_{600} of about 0.3. For the estradiol-GEM inducible system (7,45), 1 μM of

329   β–estradiol was added to the media for 90 min at 30 °C. All images in the same experiments

330   were acquired with the same laser and exposure settings. For yeast 3D imaging, 0.5 μm step size

331   for 6 μm in total in Z was applied. Image processing was performed using ImageJ software

332   (NIH). For visualization purposes, images were scaled with bilinear interpolation and shown as

333   the middle Z panel or maximum intensity projection (MIP) on Z for individual or merged

334   fluorescent channels.

335

336   **Super resolution imaging**

337   Structured illumination microscopy (SIM) images were acquired with a GE OMX-SR Super-

338   Resolution Microscope 3D Structure Illumination (3D-SIM) equipped with high-sensitivity PCO

339   sCMOS cameras. GFP and mCherry were excited with 488 nm and 568 nm lasers, respectively.

340   The SIM images were reconstructed with the Softworx and aligned following the Applied

341   Precision protocols. 3D rendering was performed with Imaris (Oxford Instruments Group).

342

343   **Split-GFP quantification**

344   Split-GFP fluorescence from confocal images was quantified by using a custom Python code

345   described before (6). In brief, mCherry and GFP intensities were summed along the Z axis, and

346   then subjected to a random walk segmentation of the background and watershed segmentation of

347   adjoining cells. For each cell, the mCherry channel was thresholded at 5% of maximal value to

16

348   detect mitochondria, and median GFP intensity within mitochondria was calculated as the spGFP

349   intensity per cell. Mean spGFP intensities of at least three biological repeats were used for the

350   following analyses. Quantifications were shown either in absolute intensity values with an

351   arbitrary unit or as normalized spGFP intensities to highlight the relative changes from the wild-

352   type cells.

353

354   **Yeast whole cell lysis and immunoblots**

355   Yeast cells in the indicated background were collected by centrifugation and snap frozen in

356   liquid nitrogen for storage. Pellets were disrupted, boiled in 120 μl LDS sample buffer with 40

357   mM DTT (Thermo) for 10 min, and vortexed with an equal volume of 0.5 mm acid-washed glass

358   beads to break cells at 4 °C for 2 min with 1 min interval. Cell lysates were re-boiled for 5 min,

359   separated from glass beads by 15,000 g centrifugation at room temperature for 30 sec, and

360   analyzed by SDS-PAGE.

361

362   Gel transfer was performed in iBlot2 (Thermo) and immunoblots were developed using Clarity

363   Western ECL substrate (Bio-Rad) for HRP-linked secondary antibodies, or directly using

364   fluorescent IRDye secondary antibodies (LI-COR). Data were acquired by using LI-COR

365   imaging system and analyzed in Image Studio (LI-COR). HA-tag (C29F4) rabbit mAb #3724

366   from Cell Signaling Technology. PGK1 mouse mAb (22C5D8) from Invitrogen. GFP Living

367   Colors A.v. mAb clone JL-8 (632381) from Takara Bio. Ubiquitin mouse mAb (P4D1) from

368   Santa Cruz Biotechnology. Gas1 (N-terminal) antiserum was kindly provided by Dr. Hongyi Wu

369   at the Mechanobiology Institute, NUS, Singapore.

370

17

Mig1 nucleocytoplasmic translocation

Nucleocytoplasmic distribution of Mig1-GFP was quantified using a custom ImageJ macro and

MATLAB script as published previously (46). Nuclear protein Pus1-RFP was used to create

nucleoplasmic mask for the individual cell. Cytoplasm was defined by a dilated nuclear mask.

The nuclear-cytoplasmic ratio of each cell was calculated by dividing the mean nuclear intensity

by the mean cytoplasmic intensity. Populational means nuclear-cytoplasmic ratio of at least three

biological replicates were used for statistical analyses.

Yeast spotting assay

Single colonies of wild-type and mutant cells were inoculated in YPD media at 30 °C overnight.

The cultures were diluted to the same OD_{600} of 1 and spotted at 10× serial dilutions from left to

right on YPD plates containing 0.01% DMSO as control or 10 μg/ml CFW. Plates were then

incubated at 30 °C for at least 2.5 days before scanning.

Cycloheximide chase assay

Degradation of endogenous Lsg1 proteins after heat shock was evaluated as described previously

(6). Briefly, a log-phase culture of yeast expressing Lsg1-HA was heated at 42 °C for 30 min.

Recovery at 30 °C was performed in the presence of 100 μg/ml cycloheximide (CHX). At the

indicated time points, the same volume of culture was collected, lysed by boiling and glass bead

beating in LDS sample buffer, and subjected to immunoblotting analysis. To assess the UPS-

mediated degradation, Ub-R-EGFP expression was induced in the presence of 1 mM $CuSO_4$ for

30 min at 30 °C, followed by treatment with 100 μg/ml cycloheximide for 1 h. Single-cell GFP

18

393   fluorescence was measured by using Attune NxT flow cytometer equipped with appropriate filter

394   sets. Mean single-cell GFP intensities of three biological repeats were quantified and plotted.

395

396   **Hydropathy plots**

397   Kyte-Doolittle hydropathy plots were generated using ProtScale (47,48) and the following

398   parameters: window size, 5 amino acids; relative weight of the window edges compared to the

399   window center, 100 %; linear weight variation model; no normalization. Transmembrane domain

400   was predicted using TMHMM-2.0 (49).

401

402   **Statistical analysis**

403   Descriptions of statistical tests and *P* values can be found in Figure Legends. Statistical analyses

404   were performed with GraphPad Prism 6.0. No statistical methods were used to predetermine the

405   sample size. The experiments were not randomized, and the investigators were not blinded to

406   allocation during experiments and result assessment.

407

421

Author Contributions

423   Conceptualization, investigation, visualization, and writing: YW, LR, RL

424   Project supervision: RL

425

Competing Interests

427   The authors declare no competing interests.

428

Data and materials availability

430   All data needed to evaluate the conclusions are available in the manuscript. Additional data and

431   materials related to this study can be requested from the authors. Requests for resources and

432   reagents should be directed to and will be fulfilled by the corresponding author, RL

433   (rong@jhu.edu).

434

435

20

Reference

1. W. E. Balch, R. I. Morimoto, A. Dillin, J. W. Kelly, Adapting proteostasis for disease intervention. *Science*. **319**, 916–919 (2008).

2. J. Labbadia, R. I. Morimoto, The biology of proteostasis in aging and disease. *Annu Rev Biochem*. **84**, 435–464 (2015).

3. C. López-Otín, M. A. Blasco, L. Partridge, M. Serrano, G. Kroemer, Hallmarks of aging: An expanding universe. *Cell*. **186**, 243–278 (2023).

4. C. Pohl, I. Dikic, Cellular quality control by the ubiquitin-proteasome system and autophagy. *Science*. **366**, 818–822 (2019).

5. T. Wai, T. Langer, Mitochondrial Dynamics and Metabolic Regulation. *Trends Endocrinol Metab*. **27**, 105–117 (2016).

6. L. Ruan, C. Zhou, E. Jin, A. Kucharavy, Y. Zhang, Z. Wen, L. Florens, R. Li, Cytosolic proteostasis through importing of misfolded proteins into mitochondria. *Nature*. **543**, 443–446 (2017).

7. Y. Wang, L. Ruan, J. Zhu, X. Zhang, A. C.-C. Chang, A. Tomaszewski, Metabolic regulation of misfolded protein import into mitochondria. *bioRxiv*. 2023.03.29.534670. [accessed 2023 May 25]. https://doi.org/10.1101/2023.03.29.534670

8. L. Ruan, Y. Wang, X. Zhang, A. Tomaszewski, J. T. McNamara, R. Li, Mitochondria-Associated Proteostasis. *Annu Rev Biophys*. **49**, 41–67 (2020).

9. Y. Li, Y. Xue, X. Xu, G. Wang, Y. Liu, H. Wu, W. Li, Y. Wang, Z. Chen, W. Zhang, Y. Zhu, W. Ji, T. Xu, L. Liu, Q. Chen, A mitochondrial FUNDC1/HSC70 interaction organizes the proteostatic stress response at the risk of cell morbidity. *EMBO J*. **38**, e98786 (2019).

10. L. Devi, V. Raghavendran, B. M. Prabhu, N. G. Avadhani, H. K. Anandatheerthavarada, Mitochondrial import and accumulation of alpha-synuclein impair complex I in human dopaminergic neuronal cultures and Parkinson disease brain. *J Biol Chem*. **283**, 9089–9100 (2008).

11. J. Deng, P. Wang, X. Chen, H. Cheng, J. Liu, K. Fushimi, L. Zhu, J. Y. Wu, FUS interacts with ATP synthase beta subunit and induces mitochondrial unfolded protein response in cellular and animal models. *Proc Natl Acad Sci U S A*. **115**, E9678–E9686 (2018).

12. W. Wang, L. Wang, J. Lu, S. L. Siedlak, H. Fujioka, J. Liang, S. Jiang, X. Ma, Z. Jiang, E. L. da Rocha, M. Sheng, H. Choi, P. H. Lerou, H. Li, X. Wang, The inhibition of TDP-43 mitochondrial localization blocks its neuronal toxicity. *Nat Med*. **22**, 869–878 (2016).

13. C. Nuoffer, P. Jenö, A. Conzelmann, H. Riezman, Determinants for glycophospholipid anchoring of the Saccharomyces cerevisiae GAS1 protein to the plasma membrane. *Mol*

471   *Cell Biol*. **11**, 27–37 (1991).

472   14. L. Popolo, M. Vai, The Gas1 glycoprotein, a putative wall polymer cross-linker. *Biochim*
473   *Biophys Acta*. **1426**, 385–400 (1999).

474   15. E. Ragni, T. Fontaine, C. Gissi, J. P. Latgè, L. Popolo, The Gas family of proteins of
475   Saccharomyces cerevisiae: characterization and evolutionary analysis. *Yeast*. **24**, 297–308
476   (2007).

477   16. Q. Y. Yin, P. W. J. de Groot, L. de Jong, F. M. Klis, C. G. De Koster, Mass spectrometric
478   quantitation of covalently bound cell wall proteins in Saccharomyces cerevisiae. *FEMS*
479   *Yeast Res*. **7**, 887–896 (2007).

480   17. I. Mouyna, T. Fontaine, M. Vai, M. Monod, W. A. Fonzi, M. Diaquin, L. Popolo, R. P.
481   Hartland, J. P. Latgé, Glycosylphosphatidylinositol-anchored glucanosyltransferases play
482   an active role in the biosynthesis of the fungal cell wall. *J Biol Chem*. **275**, 14882–14889
483   (2000).

484   18. R. Gupta, P. Kasturi, A. Bracher, C. Loew, M. Zheng, A. Villella, D. Garza, F. U. Hartl, S.
485   Raychaudhuri, Firefly luciferase mutants as sensors of proteome stress. *Nat Methods*. **8**,
486   879–884 (2011).

487   19. M. J. De Vit, J. A. Waddle, M. Johnston, Regulated nuclear translocation of the Mig1
488   glucose repressor. *Mol Biol Cell*. **8**, 1603–1618 (1997).

489   20. W.-K. Huh, J. V. Falvo, L. C. Gerke, A. S. Carroll, R. W. Howson, J. S. Weissman, E. K.
490   O'Shea, Global analysis of protein localization in budding yeast. *Nature*. **425**, 686–691
491   (2003).

492   21. M. R. Koch, L. Pillus, The glucanosyltransferase Gas1 functions in transcriptional
493   silencing. *Proc Natl Acad Sci U S A*. **106**, 11224–11229 (2009).

494   22. A. F. J. Ram, F. M. Klis, Identification of fungal cell wall mutants using susceptibility
495   assays based on Calcofluor white and Congo red. *Nat Protoc*. **1**, 2253–2256 (2006).

496   23. T. L. Doering, R. Schekman, GPI anchor attachment is required for Gas1p transport from
497   the endoplasmic reticulum in COP II vesicles. *EMBO J*. **15**, 182–191 (1996).

498   24. C. Nuoffer, A. Horvath, H. Riezman, Analysis of the sequence requirements for
499   glycosylphosphatidylinositol anchoring of Saccharomyces cerevisiae Gas1 protein. *J Biol*
500   *Chem*. **268**, 10558–10563 (1993).

501   25. S. C. Kuo, J. O. Lampen, Tunicamycin--an inhibitor of yeast glycoprotein synthesis.
502   *Biochem Biophys Res Commun*. **58**, 287–295 (1974).

503   26. Y. Kimata, K. Kohno, Endoplasmic reticulum stress-sensing mechanisms in yeast and
504   mammalian cells. *Curr Opin Cell Biol*. **23**, 135–142 (2011).

27. C. Carotti, E. Ragni, O. Palomares, T. Fontaine, G. Tedeschi, R. Rodríguez, J. P. Latgé, M. Vai, L. Popolo, Characterization of recombinant forms of the yeast Gas1 protein and identification of residues essential for glucanosyltransferase activity and folding. *Eur J Biochem*. **271**, 3635–3645 (2004).

28. V. Mrsa, F. Klebl, W. Tanner, Purification and characterization of the Saccharomyces cerevisiae BGL2 gene product, a cell wall endo-beta-1,3-glucanase. *J Bacteriol*. **175**, 2102–2106 (1993).

29. S. Heessen, N. P. Dantuma, P. Tessarz, M. Jellne, M. G. Masucci, Inhibition of ubiquitin/proteasome-dependent proteolysis in Saccharomyces cerevisiae by a Gly-Ala repeat. *FEBS Lett*. **555**, 397–404 (2003).

30. A. Bachmair, D. Finley, A. Varshavsky, In vivo half-life of a protein is a function of its amino-terminal residue. *Science*. **234**, 179–186 (1986).

31. R. S. Samant, C. M. Livingston, E. M. Sontag, J. Frydman, Distinct proteostasis circuits cooperate in nuclear and cytoplasmic protein quality control. *Nature*. **563**, 407–411 (2018).

32. D. E. Levin, Cell wall integrity signaling in Saccharomyces cerevisiae. *Microbiol Mol Biol Rev*. **69**, 262–291 (2005).

33. L. Popolo, M. Vai, E. Gatti, S. Porello, P. Bonfante, R. Balestrini, L. Alberghina, Physiological analysis of mutants indicates involvement of the Saccharomyces cerevisiae GPI-anchored protein gp115 in morphogenesis and cell separation. *J Bacteriol*. **175**, 1879–1885 (1993).

34. A. F. Ram, J. C. Kapteyn, R. C. Montijn, L. H. Caro, J. E. Douwes, W. Baginsky, P. Mazur, H. van den Ende, F. M. Klis, Loss of the plasma membrane-bound protein Gas1p in Saccharomyces cerevisiae results in the release of beta1,3-glucan into the medium and induces a compensation mechanism to ensure cell wall integrity. *J Bacteriol*. **180**, 1418–1424 (1998).

35. M. Eustice, L. Pillus, Unexpected function of the glucanosyltransferase Gas1 in the DNA damage response linked to histone H3 acetyltransferases in Saccharomyces cerevisiae. *Genetics*. **196**, 1029–1039 (2014).

36. H.-J. Cui, X.-G. Cui, X. Jing, Y. Yuan, Y.-Q. Chen, Y.-X. Sun, W. Zhao, X.-G. Liu, GAS1 Deficient Enhances UPR Activity in Saccharomyces cerevisiae. *Biomed Res Int*. **2019**, 1238581 (2019).

37. T. Scrimale, L. Didone, K. L. de Mesy Bentley, D. J. Krysan, The unfolded protein response is induced by the cell wall integrity mitogen-activated protein kinase signaling cascade and is required for cell wall integrity in Saccharomyces cerevisiae. *Mol Biol Cell*. **20**, 164–175 (2009).

38. C. Andréasson, M. Ott, S. Büttner, Mitochondria orchestrate proteostatic and metabolic stress responses. *EMBO Rep*. **20**, e47865 (2019).

39. C. Zhou, B. D. Slaughter, J. R. Unruh, F. Guo, Z. Yu, K. Mickey, A. Narkar, R. T. Ross, M. McClain, R. Li, Organelle-based aggregation and retention of damaged proteins in asymmetrically dividing cells. *Cell*. **159**, 530–542 (2014).

40. S. Escusa-Toret, W. I. M. Vonk, J. Frydman, Spatial sequestration of misfolded proteins by a dynamic chaperone pathway enhances cellular fitness during stress. *Nat Cell Biol*. **15**, 1231–1243 (2013).

41. T. Ast, G. Cohen, M. Schuldiner, A network of cytosolic factors targets SRP-independent proteins to the endoplasmic reticulum. *Cell*. **152**, 1134–1145 (2013).

42. I. Yofe, U. Weill, M. Meurer, S. Chuartzman, E. Zalckvar, O. Goldman, S. Ben-Dor, C. Schütze, N. Wiedemann, M. Knop, A. Khmelinskii, M. Schuldiner, One library to make them all: streamlining the creation of yeast libraries via a SWAp-Tag strategy. *Nat Methods*. **13**, 371–378 (2016).

43. G. Giaever, A. M. Chu, L. Ni, C. Connelly, L. Riles, S. Véronneau, S. Dow, A. Lucau-Danila, K. Anderson, B. André, A. P. Arkin, A. Astromoff, M. El-Bakkoury, R. Bangham, R. Benito, S. Brachat, S. Campanaro, M. Curtiss, K. Davis, A. Deutschbauer, K.-D. Entian, P. Flaherty, F. Foury, D. J. Garfinkel, M. Gerstein, D. Gotte, U. Güldener, J. H. Hegemann, S. Hempel, Z. Herman, D. F. Jaramillo, D. E. Kelly, S. L. Kelly, P. Kötter, D. LaBonte, D. C. Lamb, N. Lan, H. Liang, H. Liao, L. Liu, C. Luo, M. Lussier, R. Mao, P. Menard, S. L. Ooi, J. L. Revuelta, C. J. Roberts, M. Rose, P. Ross-Macdonald, B. Scherens, G. Schimmack, B. Shafer, D. D. Shoemaker, S. Sookhai-Mahadeo, R. K. Storms, J. N. Strathern, G. Valle, M. Voet, G. Volckaert, C. Wang, T. R. Ward, J. Wilhelmy, E. A. Winzeler, Y. Yang, G. Yen, E. Youngman, K. Yu, H. Bussey, J. D. Boeke, M. Snyder, P. Philippsen, R. W. Davis, M. Johnston, Functional profiling of the Saccharomyces cerevisiae genome. *Nature*. **418**, 387–391 (2002).

44. E. A. Costa, K. Subramanian, J. Nunnari, J. S. Weissman, Defining the physiological role of SRP in protein-targeting efficiency and specificity. *Science*. **359**, 689–692 (2018).

45. C. H. Ho, L. Magtanong, S. L. Barker, D. Gresham, S. Nishimura, P. Natarajan, J. L. Y. Koh, J. Porter, C. A. Gray, R. J. Andersen, G. Giaever, C. Nislow, B. Andrews, D. Botstein, T. R. Graham, M. Yoshida, C. Boone, A molecular barcoded yeast ORF library enables mode-of-action analysis of bioactive compounds. *Nat Biotechnol*. **27**, 369–377 (2009).

46. J. B. Kelley, B. M. Paschal, Fluorescence-based quantification of nucleocytoplasmic transport. *Methods*. **157**, 106–114 (2019).

47. J. Kyte, R. F. Doolittle, A simple method for displaying the hydropathic character of a protein. *J Mol Biol*. **157**, 105–132 (1982).

48. E. Gasteiger, C. Hoogland, A. Gattiker, S. Duvaud, M. R. Wilkins, R. D. Appel, A. Bairoch, "Protein Identification and Analysis Tools on the ExPASy Server" in *The Proteomics Protocols Handbook*, J. M. Walker, Ed. (Humana Press, Totowa, NJ, 2005; http://link.springer.com/10.1385/1-59259-890-0:571), pp. 571–607.

24

580   49.   S. Möller, M. D. Croning, R. Apweiler, Evaluation of methods for the prediction of
581   membrane spanning regions. *Bioinformatics*. **17**, 646–653 (2001).
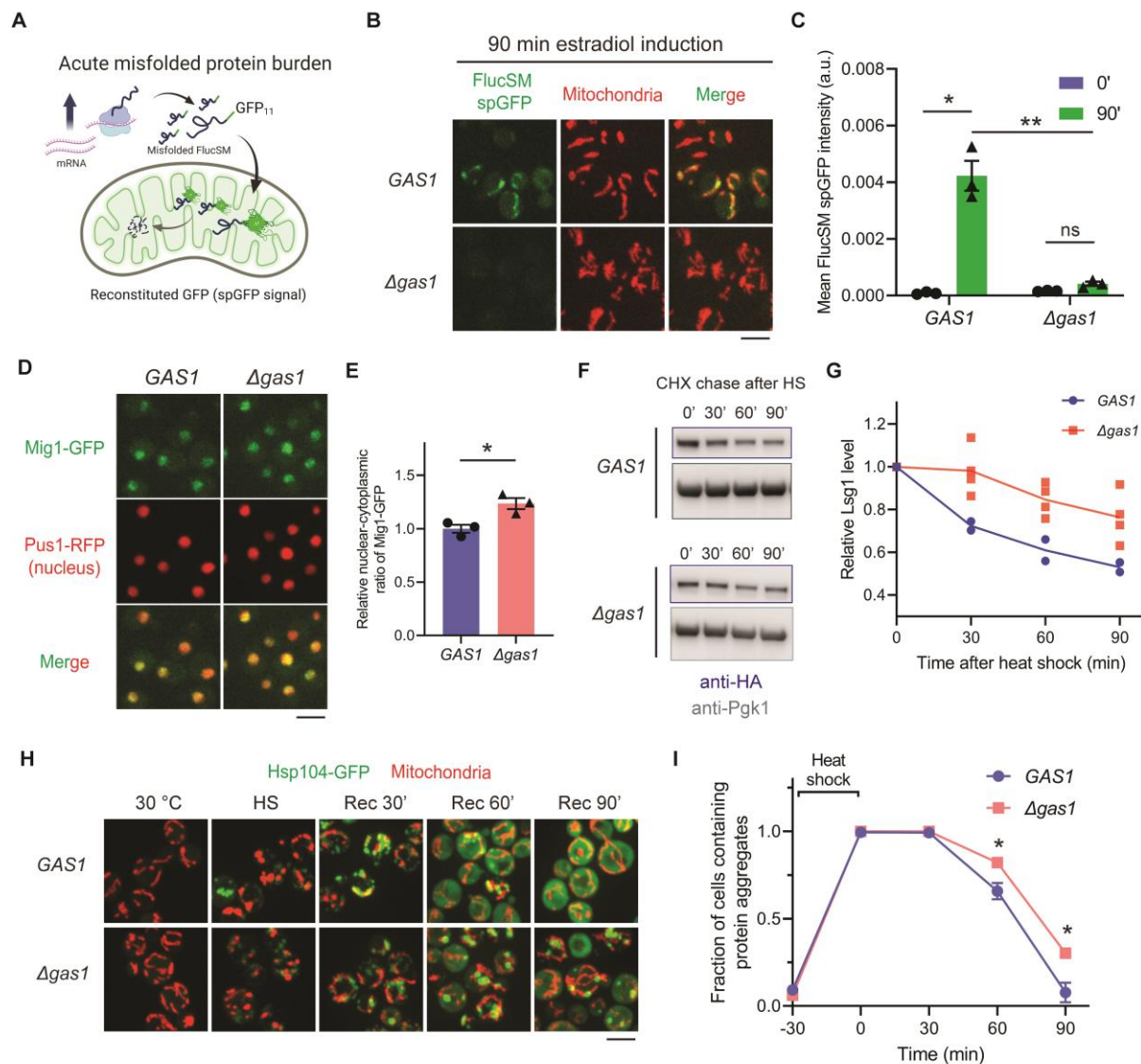
582

583

Figure 1

584

Figure 1. Loss of Gas1 inhibits mitochondrial accumulation and degradation of misfolded proteins.

(**A**) Schematic diagram of FlucSM split-GFP assay upon proteotoxic stress associated with elevated

misfolded protein burden. (**B**, **C**) Images (B) and quantification (C) of FlucSM spGFP signal in

mitochondria of wild-type *GAS1* and *Δgas1* cells after estradiol induction. Shown in (C): means ± SEM of

FlucSM spGFP intensities with arbitrary unit (a.u.). Paired two-tailed *t*-test between no induction (0') and

90 min induction (90'). Unpaired two-tailed *t*-test between *GAS1* and *Δgas1* cells after 90 min induction.

Three biological repeats. (**D**, **E**) Images (D) and quantification (E) of the nuclear-cytoplasmic

translocation of Mig1-GFP signal. Shown in (E): means ± SEM of normalized Mig-GFP nuclear-

26

593   cytoplasmic ratios. Unpaired two-tailed *t*-test. (**F**, **G**) Immunoblots (F) and quantifications (G) showing

594   data points and means of Lsg1-HA degradation *in vivo* after heat shock (HS) in the presence of

595   cycloheximide (CHX). (**H, I**) Dissolution of protein aggregates labeled with Hsp104-GFP in *GAS1* and

596   *Δgas1* cells during recovery (Rec) after heat shock. Shown in (I): means ± SEM of fractions of cells

597   containing protein aggregates. Unpaired two-tailed *t*-test. *$P < 0.05$; **$P < 0.01$; ***$P < 0.001$; ns, not
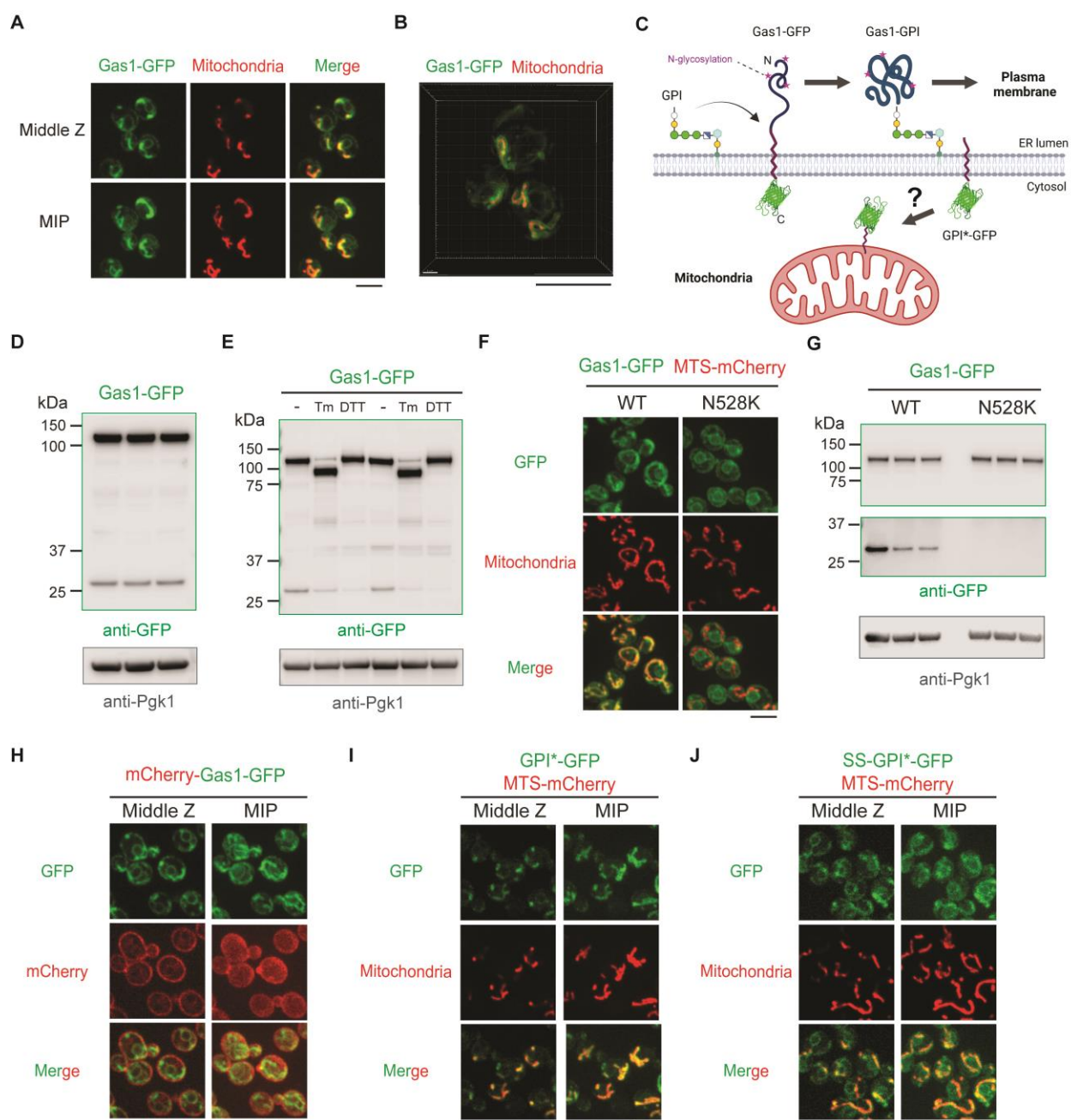
598   significant, $P > 0.05$. Scale bars, 5 μm.

599

Figure 2

Figure 2. C-terminal GPI anchor signal of Gas1 localizes to mitochondria. (**A**) Images of Gas1-GFP, showing partial colocalization with mitochondrial matrix labeled by MTS-mCherry. The ring-like structure may represent ER/nuclear periphery as reported previously (21). MIP, maximal intensity projection. (**B**) 3D rendering of super-resolution images of Gas1-GFP, showing GFP signals outside the mitochondrial matrix labeled with MTS-mCherry. (**C**) Working model of GPI addition and peptide

606   cleavage during Gas1 maturation in the ER. (**D**) Immunoblots of whole cell lysates showing two major

607   species with GFP. Three biological repeats. (**E**) Immunoblots of whole cell lysates after tunicamycin (Tm)

608   or DTT treatment. (**F, G**) Images (F) and immunoblots (G) of whole cell lysates expressing Gas1-GFP or

609   Gas1^{N528K}-GFP. (**H-J**) Images of cells expressing an ectopic copy of mCherry-Gas1-GFP (H), GPI*-GFP

610   (I), or SS-GPI*-GFP (J). MIP, maximal intensity projection. Scale bars, 5 μm.
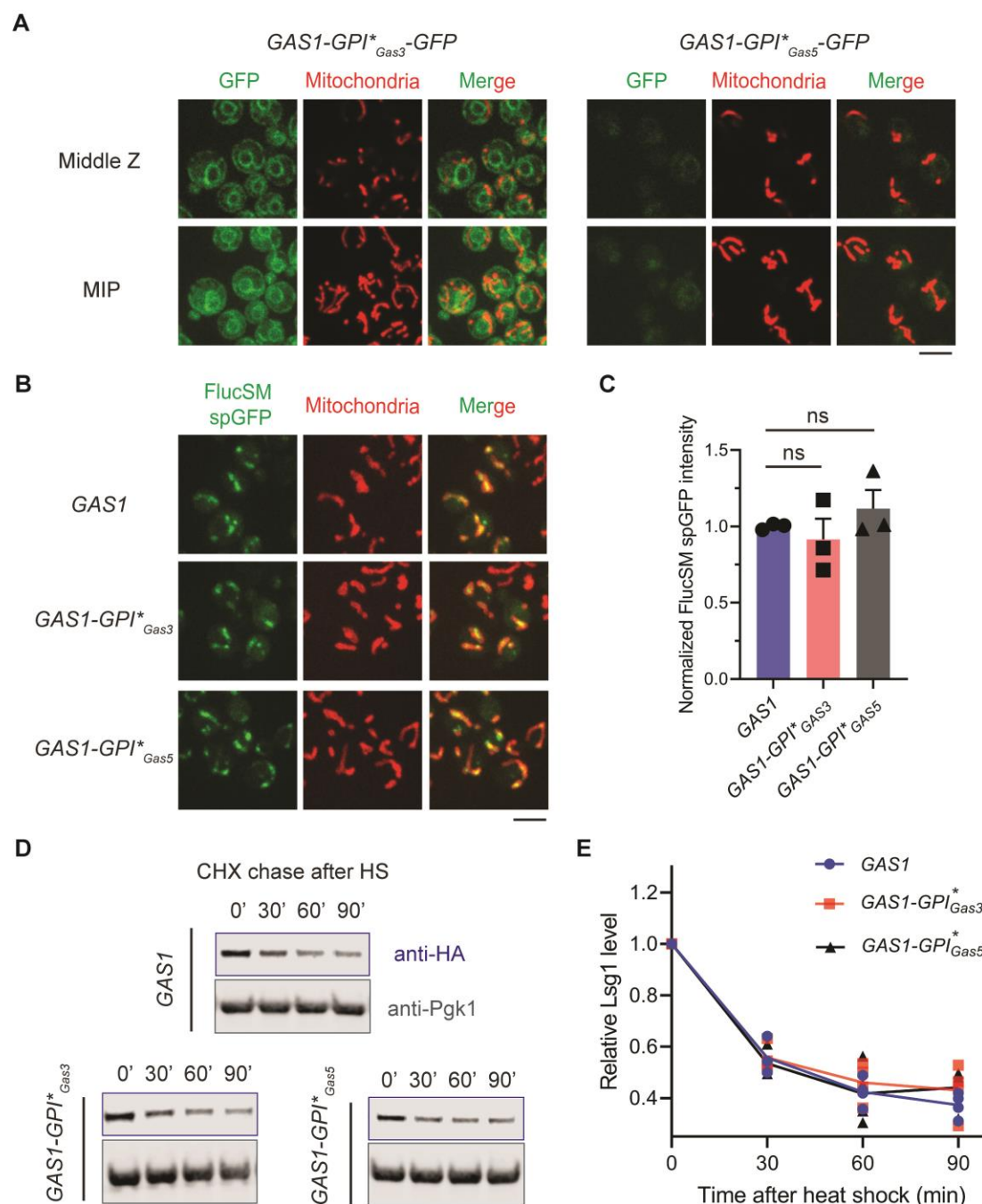
611

Figure 3

Figure 3. Mitochondria-associated GPI anchor signal of Gas1 is not required for MAGIC. (**A**) Images of cells expressing an ectopic copy of Gas1-GPI*$_{Gas3}$-GFP or Gas1-GPI*$_{Gas5}$-GFP and MTS-mCherry labelling mitochondria. MIP, maximal intensity projection. (**B, C**) Images (B) and quantification

616   (C) of FlucSM spGFP signal in mitochondria of cells expressing wild-type or recombinant Gas1 with

617   GPI* replaced. Shown in (C): means ± SEM of normalized FlucSM spGFP intensities. ns, not significant,

618   *P* > 0.05. Unpaired two-tailed *t*-test. (**D**, **E**) Immunoblots (D) and quantifications (E) of Lsg1-HA

619   degradation *in vivo* after heat shock (HS) in the presence of cycloheximide (CHX). Scale bars, 5 μm.
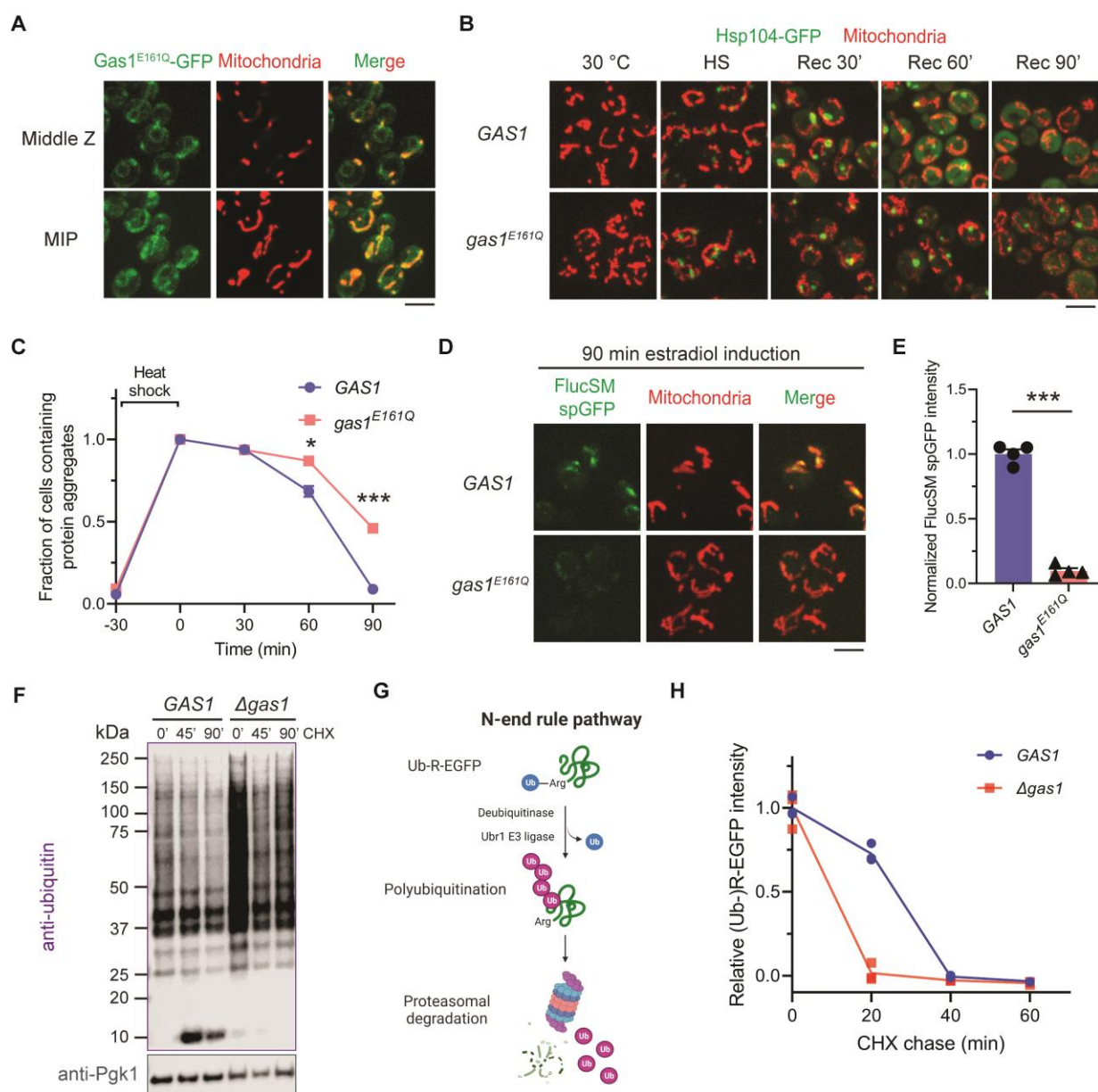
620

Figure 4

Figure 4. Loss of Gas1 activity inhibits MAGIC but elevates UPS-mediated degradation.

(**A**) Images of cells expressing an ectopic copy of Gas1^{E161Q}-GFP and MTS-mCherry. MIP, maximal

intensity projection. (**B**, **C**) Dissolution of protein aggregates labeled with Hsp104-GFP in *GAS1* and

gas1^{E161Q} cells after heat shock. Unpaired two-tailed *t*-test. (**D**, **E**) Images (D) and quantification (E) of

627   FlucSM spGFP in mitochondria of *GAS1* and *gas1^{E161Q}* cells after estradiol treatment for 90 min. Shown

628   in (E): means ± SEM of normalized FlucSM spGFP intensities. Unpaired two-tailed *t*-test. (**F**) Anti-

629   ubiquitin immunoblots of cell lysates before and after cycloheximide (CHX) treatment, showing an

630   accumulation of polyubiquitinated species with high molecular weight in *Δgas1* cells. (**G**) Diagram of N-

631   end rule pathway using Ub-R-EGFP as a proteasomal substrate. (**H**) Degradation of copper-induced Ub-

632   R-EGFP signal *in vivo* in wild-type and *Δgas1* cells. Three biological repeats. *$P < 0.05$; ***$P < 0.001$.

633   Scale bars, 5 μm.

634

Supplementary Figure 1
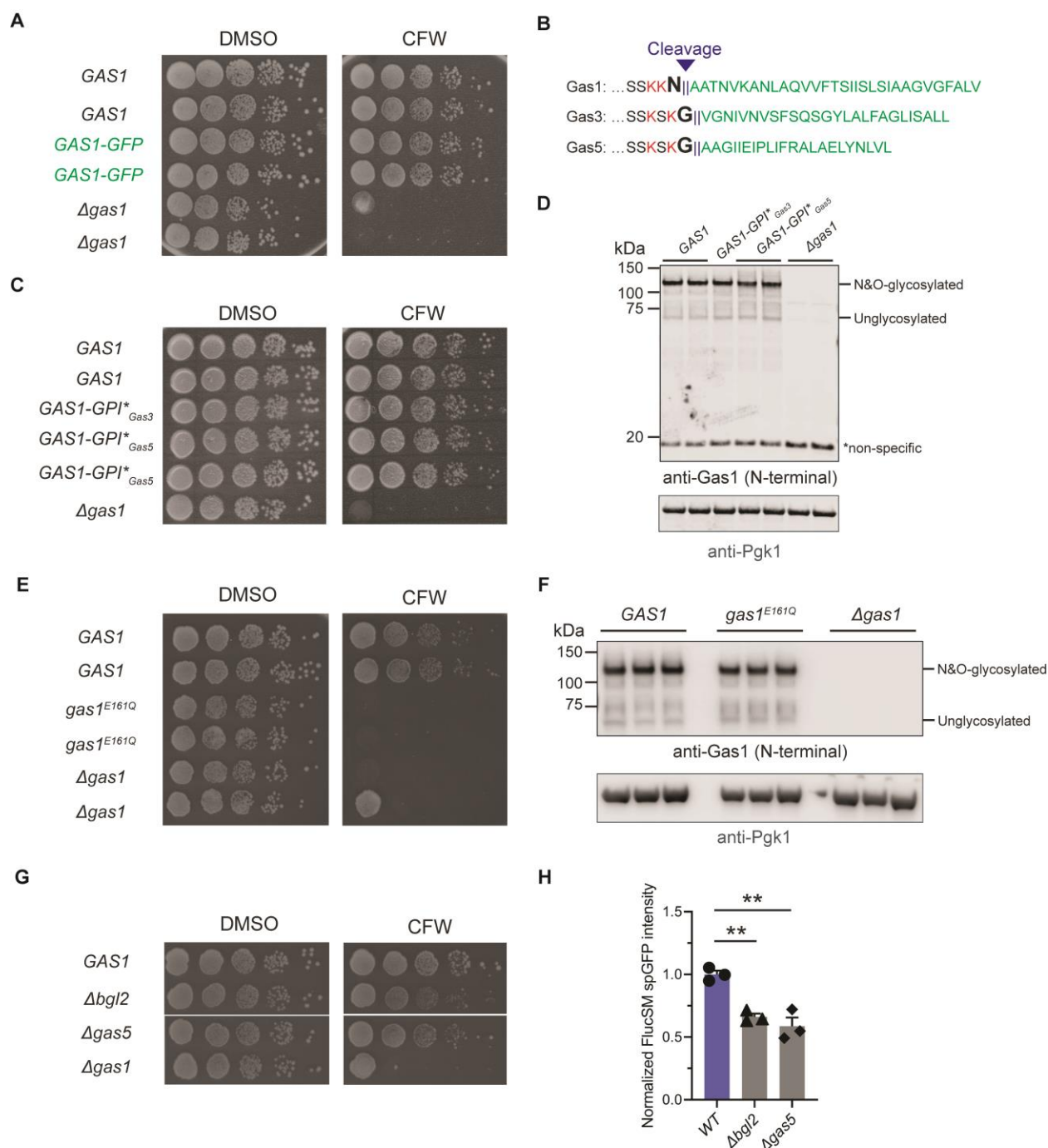
Supplementary Figure 1. Characterization of Gas1-related mutants. (A, C, E, G) Yeast spotting assays on YPD plates containing DMSO or calcofluor white (CFW). Ten-fold serial dilutions from left to right for each plate. (**B**) C-terminal sequences of three Gas family proteins. Red, key basic residues; Bold,

639   GPI-anchored attachment sites; Green, GPI anchor signals to be removed in matured proteins. (**D, F**)

640   Immunoblots of whole cell lysates with wild-type, GPI* replaced, or catalytically inactive Gas1 using

641   antiserum against the N-terminus of Gas1. (**H**) Quantification of mitochondrial FlucSM spGFP signal in

642   wild-type cells and two cell wall mutants. Means ± SEM of normalized FlucSM spGFP intensities are

643   shown. Unpaired two-tailed *t*-test. **$*P < 0.01$.

644

Supplementary Figure 2

A

645
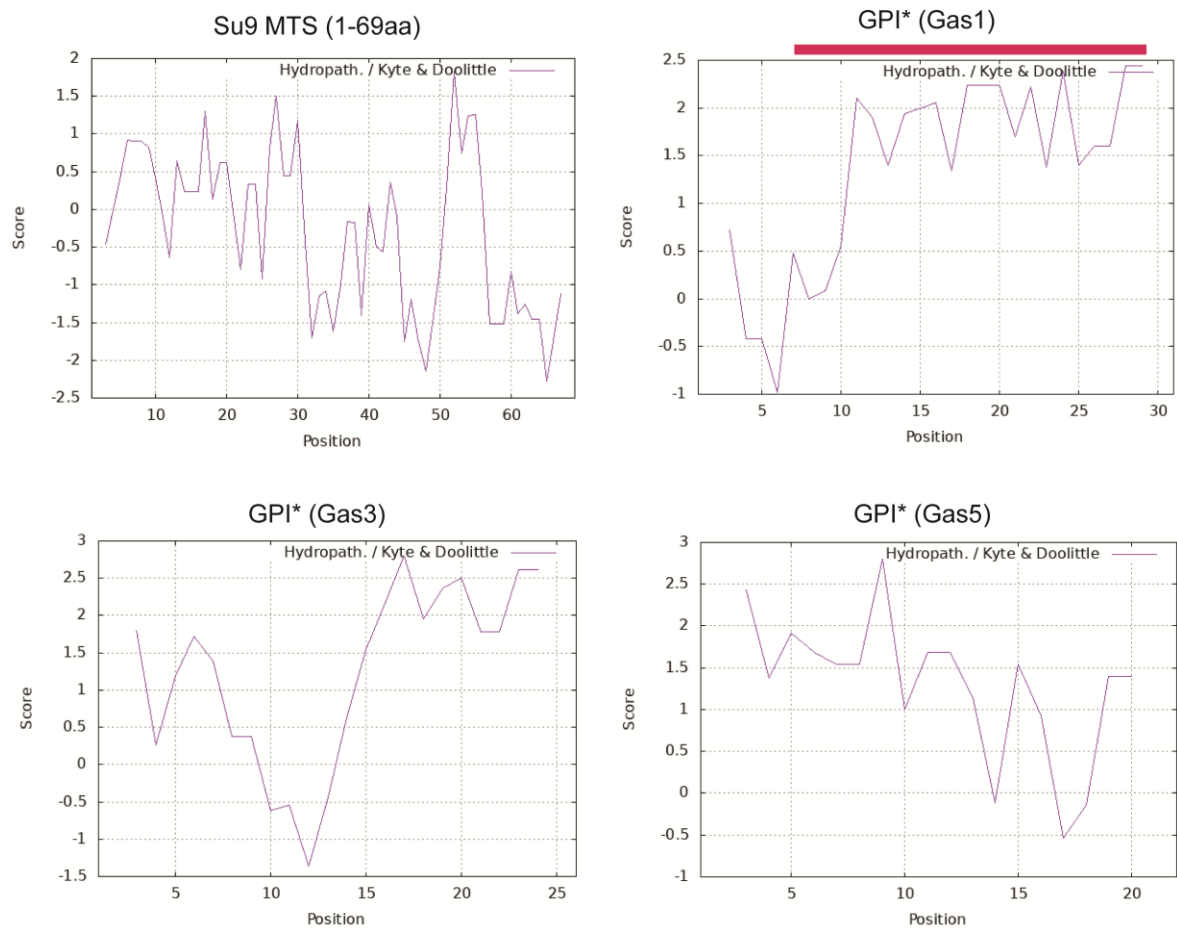
Supplementary Figure 2. Sequence analyses of Su9 MTS and GPI anchor signals. (**A**) Kyte-Doolittle

hydropathy plots generated by ProtScale. Su9 MTS is the first 69 residues of ATP synthase subunit 9 from

Neurospora crassa (primary accession: P00842). GPI* of yeast Gas1, Gas3, and Gas5 represent the GPI

anchor signal peptides. A transmembrane domain predicted by TMHMM-2.0 is highlighted as red bar.

650

651 **Table 1. List of yeast strains and plasmids**

Yeast	Genotype	Reference
BY4741	*MATa his3Δ1; leu2Δ0; met15Δ0; ura3Δ0*	
RLY9803	*trp1::P_{GPD}-GRX5-HA-GFP$_{1-10}$-natMX6; amp::GEM-P_{GAL1}-FlucSM-HA-GFP$_{11}$-kanMX6; TOM70-mCherry-Ura3MX6*	7
RLY9806	*MIG1-GFP-His3MX6; PUS1-RFP-hphMX6*	7
RLY9860	*trp1::P_{GPD}-GRX5-HA-GFP$_{1-10}$-natMX6; amp::GEM-P_{GAL1}-FlucSM-HA-GFP$_{11}$-kanMX6; TOM70-mCherry-Ura3MX6; Δgas1-his3MX6*	
RLY9861	*MIG1-GFP-His3MX6; PUS1-RFP-hphMX6; Δgas1-Leu2*	
RLY9862	*trp1::P_{GPD}-MTS-mCherry-GFP$_{1-10}$-natMX6; LSG1-HA-GFP$_{11}$-hisMX6*	
RLY9863	*trp1::P_{GPD}-MTS-mCherry-GFP$_{1-10}$-natMX6; LSG1-HA-GFP$_{11}$-hisMX6; Δgas1-kanMX6*	
RLY9864	*HSP104-GFP-his3MX6; trp1::P_{GPD}-MTS-mCherry-natMX6*	6
RLY9865	*HSP104-GFP-his3MX6; trp1::P_{GPD}-MTS-mCherry-natMX6; Δgas1-kanMX6*	
RLY9866	*GAS1-GFP-his3MX6*	20
RLY9867	*GAS1-GFP-his3MX6; trp1::P_{GPD}-MTS-mCherry-natMX6*	
RLY9868	*Δgas1-kanMX6*	
RLY9869	*HO::P_{GAS1}-gas1^{N528K}-GFP-hphMX6; trp1::P_{GPD}-MTS-mCherry-natMX6*	
RLY9870	*Δgas1-kanMX6; HO::P_{GAS1}-mCherry-GAS1-GFP-his3MX6-hphMX6*	
RLY9871	*HO::P_{GAS1}-GPI*-GFP-hphMX6; trp1::P_{GPD}-MTS-mCherry-natMX6*	
RLY9872	*HO::P_{GAS1}-SS-GPI*-GFP-hphMX6; trp1::P_{GPD}-MTS-mCherry-natMX6*	
RLY9873	*GAS1-GPI*$_{GAS3}$-kanMX6*	
RLY9874	*GAS1-GPI*$_{GAS5}$-kanMX6*	
RLY9875	*GAS1-GPI*$_{GAS3}$-GFP-his3MX6-kanMX6; trp1::P_{GPD}-MTS-mCherry-natMX6*	
RLY9876	*GAS1-GPI*$_{GAS5}$-GFP-his3MX6-kanMX6; trp1::P_{GPD}-MTS-mCherry-natMX6*	
RLY9877	*trp1::P_{GPD}-MTS-mCherry-GFP$_{1-10}$-natMX6; LSG1-HA-GFP$_{11}$-hisMX6; GAS1-GPI*$_{GAS3}$-kanMX6*	
RLY9878	*trp1::P_{GPD}-MTS-mCherry-GFP$_{1-10}$-natMX6; LSG1-HA-GFP$_{11}$-hisMX6; GAS1-GPI*$_{GAS5}$-kanMX6*	

RLY9879	*HSP104-GFP-his3MX6; trp1::P_{GPD}-MTS-mCherry-natMX6; Δgas1-kanMX6-Leu2-P_{GAS1}-gas1^{E161Q}*	
RLY9880	*HO::P_{GAS1}-gas1^{E161Q}-GFP-hphMX6; trp1::P_{GPD}-MTS-mCherry-natMX6*	
RLY9881	*trp1::P_{GPD}-GRX5-HA-GFP_{1-10}-natMX6; amp::GEM-P_{GAL1}-FlucSM-HA-GFP_{11}-kanMX6; TOM70-mCherry-Ura3MX6; Δgas1-his3MX6; kanMX6-Leu2-P_{GAS1}-gas1^{E161Q}*	
RLY9882	*trp1::P_{CUP1}-Ub-R-EGFP-natMX6*	
RLY9883	*trp1::P_{CUP1}-Ub-R-EGFP-natMX6; Δgas1-kanMX6*	
RLY9884	*Δbgl2-kanMX6*	43
RLY9885	*Δgas5-kanMX6*	43
RLY9886	*ura3Δ0::GEM-hphMX6; trp1::P_{GPD}-GRX5-HA-GFP_{1-10}-natMX6; HO::P_{GAL1}-FlucSM-HA-GFP_{11}-His3MX6; TOM70-mCherry-Ura3MX6*	6
RLY9887	*ura3Δ0::GEM-hphMX6; trp1::P_{GPD}-GRX5-HA-GFP_{1-10}-natMX6; HO::P_{GAL1}-FlucSM-HA-GFP_{11}-His3MX6; TOM70-mCherry-Ura3MX6; Δbgl2-kanMX6*	
RLY9888	*ura3Δ0::GEM-hphMX6; trp1::P_{GPD}-GRX5-HA-GFP_{1-10}-natMX6; HO::P_{GAL1}-FlucSM-HA-GFP_{11}-His3MX6; TOM70-mCherry-Ura3MX6; Δgas5-kanMX6*	
RLY9889	*ura3Δ0::GEM-hphMX6; trp1::P_{GPD}-GRX5-HA-GFP_{1-10}-natMX6; HO::P_{GAL1}-FlucSM-HA-GFP_{11}-His3MX6; TOM70-mCherry-Ura3MX6; GAS1-GPI*_{GAS3}-kanMX6*	
RLY9890	*ura3Δ0::GEM-hphMX6; trp1::P_{GPD}-GRX5-HA-GFP_{1-10}-natMX6; HO::P_{GAL1}-FlucSM-HA-GFP_{11}-His3MX6; TOM70-mCherry-Ura3MX6; GAS1-GPI*_{GAS5}-kanMX6*	
Plasmid	**Sequence**	**Reference**
RLB918	*TRP1::P_{GPD}-MTS-mCherry-natMX6*	6
RLB1051	*GEM-P_{GAL1}-FlucSM-HA-GFP_{11}-KanMX6*	7
RLB1075	*pRS316-HO(homology)-P_{GAS1}-gas1^{N528K}-GFP-hphMX6-HO(homology)*	
RLB1076	*pRS316-HO(homology)-P_{GAS1}-mCherry-GAS1-hphMX6-HO(homology)*	
RLB1077	*pRS316-HO(homology)-P_{GAS1}-GPI*-GFP-hphMX6-HO(homology)*	
RLB1078	*pRS316-HO(homology)-P_{GAS1}-SS-GPI*-GFP-hphMX6-HO(homology)*	
RLB1079	*P_{GAS1}-gas1^{E161Q}-Leu2-KanMX6*	

RLB1080	*TRP1::P$_{CUP1}$-Ub-R-EGFP-natMX6*	
RLB1081	*pRS316-HO(homology)-P$_{GAS1}$-gas1^{E161Q}-GFP-hphMX6-HO(homology)*	

652